Discretization of continuous convolution operators for accurate modeling of wave propagation in digital holography

Nikhil Chacko,[1] Michael Liebling,[1,*] and Thierry Blu[2]

[1]*Department of Electrical and Computer Engineering, University of California, Santa Barbara, California 93106-9650, USA*

[2]*Department of Electronic Engineering, The Chinese University of Hong Kong, Shatin, N.T., Hong Kong, China*

**Corresponding author: liebling@ece.ucsb.edu*

Received May 10, 2013; accepted August 8, 2013;
posted August 23, 2013 (Doc. ID 190360); published September 18, 2013

Discretization of continuous (analog) convolution operators by direct sampling of the convolution kernel and use of fast Fourier transforms is highly efficient. However, it assumes the input and output signals are band-limited, a condition rarely met in practice, where signals have finite support or abrupt edges and sampling is nonideal. Here, we propose to approximate signals in analog, shift-invariant function spaces, which do not need to be band-limited, resulting in discrete coefficients for which we derive discrete convolution kernels that accurately model the analog convolution operator while taking into account nonideal sampling devices (such as finite fill-factor cameras). This approach retains the efficiency of direct sampling but not its limiting assumption. We propose fast forward and inverse algorithms that handle finite-length, periodic, and mirror-symmetric signals with rational sampling rates. We provide explicit convolution kernels for computing coherent wave propagation in the context of digital holography. When compared to band-limited methods in simulations, our method leads to fewer reconstruction artifacts when signals have sharp edges or when using nonideal sampling devices.

OCIS codes: (070.0070) Fourier optics and signal processing; (090.1995) Digital holography; (070.7345) Wave propagation; (100.2000) Digital image processing; (110.7410) Wavelets.

http://dx.doi.org/10.1364/JOSAA.30.002012

1. INTRODUCTION

Continuous convolution operations are central to model many optical systems and physical phenomena, such as wave propagation and diffraction, with applications ranging from optical image formation to digital holography and X-ray scattering [1–4]. However, since computers can only handle discrete signals, implementation of such continuous convolution operators requires an accurate mechanism to switch between analog and discrete signals.

Convolution operations are commonly discretized by sampling both the analog input signal and the convolution kernel, with classical sampling theory justifying this approach when the signals at hand are band-limited [5]. However, such an approach suffers from multiple drawbacks. First, most practical signals are not well approximated by band-limited signals, especially when they have finite support or sharp edges, leading to Gibbs oscillations. Second, traditional approaches offer little flexibility regarding the sampling rates of the input and output signals. Third, from a practical perspective, sampling devices, such as digital cameras, gather light over extended areas as opposed to infinitely small points assumed in the ideal sampling model.

Here, we address the problem of approximating continuous convolution operations within the context of generalized sampling theory [6–8], where analog signals are represented by linear combinations of shifted basis functions that need not be band-limited. The expansion coefficients in such representations are spatially localized and correspond to discrete signals that can readily be processed by a computer. The formalism also accommodates band-limited signals and therefore includes the traditional approach as a special case. However, in addition to the slow-decaying sinc function—the underlying building block tied to band-limited signals—a variety of basis functions can be used to model analog signals with finite support or discontinuities (e.g., piece-wise constant signals).

Our approach consists of (a) approximating the input signal in an analog space using shifted basis functions adapted to the signal, (b) computing an exact *analog* convolution, and (c) sampling the result by approximating (projecting) it again using suitable basis functions. This allows characterizing the input and output signals by a set of discrete coefficients, which are related by a *discrete* convolution. The design, therefore, retains the efficiency of the traditional approach and can readily be implemented using fast Fourier transforms (FFTs).

While our approach applies to any general convolution operator, we focus on operators related to wave propagation problems. Specifically, we consider scalar diffraction theory for wave propagation, the Rayleigh–Sommerfeld diffraction integral and its Fresnel approximation [1,2]. In this context, sampling strategies have been explored previously for Fresnel fields [9–12] and more general classes of transforms that include the Fresnel transform (FrT) as a special case [13–15]. In the particular case of the FrT, implementations are either

convolution-based or involve two chirp multiplications and a single FFT [3,4], the latter thereby providing some computational advantage (though applicable only in the far-field region [16–18]). The single FFT approach also has its input and output sampling rates as parameter-dependent variants. Methods to address this issue [19,20] require zero-padding the original signal and thereby offset the computational advantage of the approach. The generalized form of the *convolution-based* approach, which we propose in this paper, is related to the Fresnelet formalism [21], with which it shares the basis function representation. Here, however, we do not require that the underlying functions yield multiresolution spaces.

The paper is organized as follows. In Section 2, we introduce the challenges related to discretizing continuous convolution operations, specifically in the context of coherent propagation of monochromatic scalar wave fields. We derive our method in Section 3 and discuss its applicability to digital holography in Section 4. In Section 5, we evaluate our algorithm in a series of simulation experiments and conclude in Section 6.

2. PROBLEM FORMULATION

We consider linear and shift-invariant (SI) systems, characterized by an impulse response, $h(\mathbf{x})$, $\mathbf{x} = (x, y) \in \mathbb{R}^2$, where the output $g(\mathbf{x})$ is given by the continuous-space (analog) convolution between the complex-valued input signal $f(\mathbf{x})$ and $h(\mathbf{x})$ as

$$g(\mathbf{x}) = \int_{\mathbb{R}^2} f(\xi) \cdot h(\mathbf{x} - \xi) \mathrm{d}\xi \triangleq f \bigstar h(\mathbf{x}). \tag{1}$$

When f is band-limited, with maximal frequency less than $1/(2\Delta x)$ and $1/(2\Delta y)$ in the x and y directions, respectively, it is possible to retrieve samples of the continuous convolution, $g[\mathbf{k}] = g(k\Delta x, \ell\Delta y)$ from uniformly spaced samples of f, $f[\mathbf{k}] = f(k\Delta x, \ell\Delta y)$, $\mathbf{k} = [k, \ell] \in \mathbb{Z}^2$, via the discrete convolution

$$g[\mathbf{k}] = \sum_{\mathbf{m} \in \mathbb{Z}^2} f[\mathbf{m}] \cdot h_{\mathrm{BL}}[\mathbf{k} - \mathbf{m}] \triangleq f * h_{\mathrm{BL}}[\mathbf{k}], \tag{2}$$

where $h_{\mathrm{BL}}[\mathbf{k}] = h_{\mathrm{BL}}(k\Delta x, \ell\Delta y)$ and

$$h_{\mathrm{BL}}(\mathbf{x}) = \frac{1}{\Delta x \Delta y} [h(\mathbf{x}) \bigstar \mathrm{sinc}(x/\Delta x)\mathrm{sinc}(y/\Delta y)] \tag{3}$$

is a band-limited version of $h(x)$. However, this straightforward implementation no longer holds if f is not band-limited. In this paper, we consider samples of functions f that are not necessarily band-limited, and use them to estimate samples of g. Our approach retains the general form of a discrete convolution as in Eq. (2), but we replace $h_{\mathrm{BL}}[\mathbf{k}]$ by a digital filter that is ideally adapted to the problem.

Before proceeding further, we recall the definitions of the scalar wave propagation operators. The Rayleigh–Sommerfeld diffraction integral [2], which relates the scalar field of a propagating wave (having wavelength λ) across two parallel planes separated by a distance z, is a convolution operation as in Eq. (1), with the kernel

$$h_{\mathrm{RS},\lambda,z}(\mathbf{x}) = \frac{z}{j\lambda} \cdot \frac{\exp\left(j\frac{2\pi}{\lambda}\sqrt{\|\mathbf{x}\|^2 + z^2}\right)}{\|\mathbf{x}\|^2 + z^2}, \tag{4}$$

whose frequency response is given by [2]

$$\hat{h}_{\mathrm{RS},\lambda,z}(\nu) = \exp\left(j2\pi z\sqrt{\frac{1}{\lambda^2} - \|\nu\|^2}\right), \qquad \nu = (\nu_x, \nu_y). \tag{5}$$

In the Fresnel approximation, h has the form [2]

$$h_{\mathrm{FrA},\lambda,z}(\mathbf{x}) = \frac{\exp\left(j\frac{2\pi}{\lambda}z\right)}{j\lambda z} \cdot \exp\left(\frac{j\pi}{\lambda z}\|\mathbf{x}\|^2\right), \tag{6}$$

which, unlike the Rayleigh–Sommerfeld kernel $h_{\mathrm{RS},\lambda,z}$, is separable:

$$h_{\mathrm{FrA},\lambda,z}(\mathbf{x}) = -j \exp\left(j\frac{2\pi}{\lambda}z\right) \cdot h_{\mathrm{FrT},\tau}(x) \cdot h_{\mathrm{FrT},\tau}(y), \tag{7}$$

where the 1D kernel $h_{\mathrm{FrT},\tau}(x)$, with its associated parameter $\tau = \sqrt{\lambda z}$, is defined as

$$h_{\mathrm{FrT},\tau}(x) = \begin{cases} \exp\left(j\frac{\pi}{4}\right) \cdot \delta(x), & \tau = 0 \\ \frac{1}{\tau}\exp\left(j\pi\frac{x^2}{\tau^2}\right), & \text{otherwise} \end{cases} \tag{8}$$

with its frequency response given by

$$\hat{h}_{\mathrm{FrT},\tau}(\nu) = \exp\left(j\frac{\pi}{4}\right) \cdot \exp(-j\pi\tau^2\nu^2), \qquad \nu \in \mathbb{R}. \tag{9}$$

This leads to the definition of the unitary 1D FrT [21] of f:

$$\tilde{\mathcal{F}}_\tau\{f\}(x) = \tilde{f}_\tau(x) = f \bigstar h_{\mathrm{FrT},\tau}(x), \qquad x \in \mathbb{R}. \tag{10}$$

Being a unitary transform, the convolution kernel and the frequency response for the inverse FrT are given by the complex conjugates, $h^{-1}_{\mathrm{FrT},\tau}(x) = h^*_{\mathrm{FrT},\tau}(x)$ and $\hat{h}^{-1}_{\mathrm{FrT},\tau}(\nu) = \hat{h}^*_{\mathrm{FrT},\tau}(\nu)$, respectively.

When f is band-limited, discretizing the wave propagation problem via Eq. (3), using the frequency spectrum of the associated convolution kernel, is known by different names in literature, including the *angular-spectrum* method and the *convolution* (CV)-based method [16–19]. In the rest of the paper, we refer to such a discretization of any convolution operation using FFT as CV-FFT. For example, the discrete FrT associated with an N-periodic 1D input sequence, $f[k]$ (samples of f at regular intervals Δx), is computed using CV-FFT as

$$\tilde{f}_\tau^{\mathrm{CV-FFT}}[k] = \mathcal{F}_N^{-1}\{\mathcal{F}_N(f) \times U^{\mathrm{CV-FFT}}[k_0]\}[k] \tag{11}$$

for $-\lfloor N/2 \rfloor \le k, k_0 < \lceil N/2 \rceil$, where

$$U^{\mathrm{CV-FFT}}[k_0] = \mathrm{rect}(k_0/N) \times \hat{h}_{\mathrm{FrT},\tau}(k_0/(N\Delta x)), \tag{12}$$

$$\mathrm{rect}(\nu) = \begin{cases} 1, & |\nu| < \frac{1}{2} \\ 0, & \text{otherwise} \end{cases} \tag{13}$$

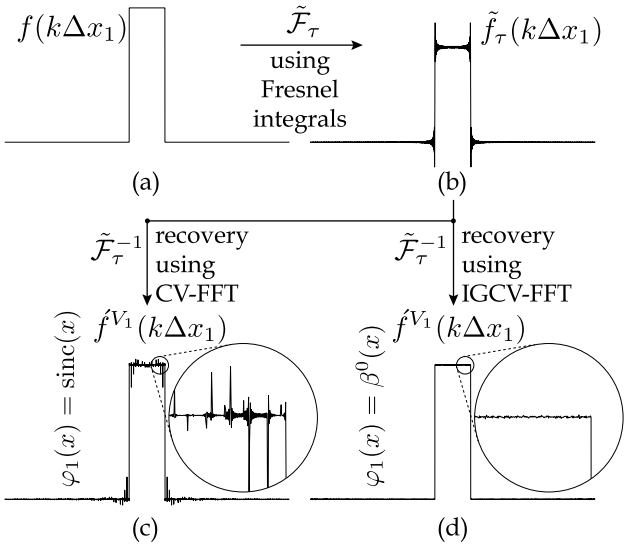

Fig. 1. (a) Box signal formed with $N = 4096$ samples where $\Delta x_1 = 10$ μm and aperture width $w = 5.15$ mm, (b) FrT computed using Fresnel integrals [22] with $\lambda = 632$ nm and $z = 5$ mm (only real values shown), (c) inverse FrT of (b) computed using CV-FFT, and (d) using IGCV-FFT where prior knowledge $(\varphi_1, \varphi_2, \Delta x_1)$ is exploited for filter design.

with $\mathcal{F}_N$ and $\mathcal{F}_N^{-1}$ referring to the forward and inverse N-point FFT, respectively. However, when the signals involved are not band-limited, such a strategy results in ringing artifacts due to the enforced band-limiting operation, as shown in Fig. 1(c), even for a near-field region where the technique is usually thought to be effective [16–18].

Finally, for the rest of this paper, we consider boundary conditions that correspond to the following two physical arrangements in the context of wave propagation: (i) free-space propagation of a periodic wave field [Fig. 2(a)], and (ii) the propagation of fields produced via transmission through or reflection by finite-sized objects confined within a rectangular waveguide lined with plane mirrors on its four interior surfaces [Fig. 2(b)]. Note that the latter is analogous to using mirror-symmetric boundaries for the computation of the discrete FrT [Fig. 2(c)].

3. PROPOSED METHOD

Our approach considers a class of functions far more general than band-limited signals. We follow the formalism of generalized sampling theory and Hilbert space projections [23], a brief review of which is given in Subsection 3.A. The basic assumptions about the functional space to which the input signal belongs are (a) integer shift-invariance, (i.e., a basis function shifted by integer-multiples of the signal's sampling step spans the space) and (b) periodicity (i.e., the signals it encompasses are periodic; the special case of aperiodic signals is covered when the period tends to infinity).

Specifically, we consider the following two problems: (P1) given the samples of a signal, f, that belongs to a known SI space, compute samples (or measurements with a known camera) of the convolution $g = f \star h$ and conversely, (P2) given measurements of $g = f \star h$, obtained with a known acquisition device, along with prior information about h and the SI space in which f lies, recover the samples of f. We discuss

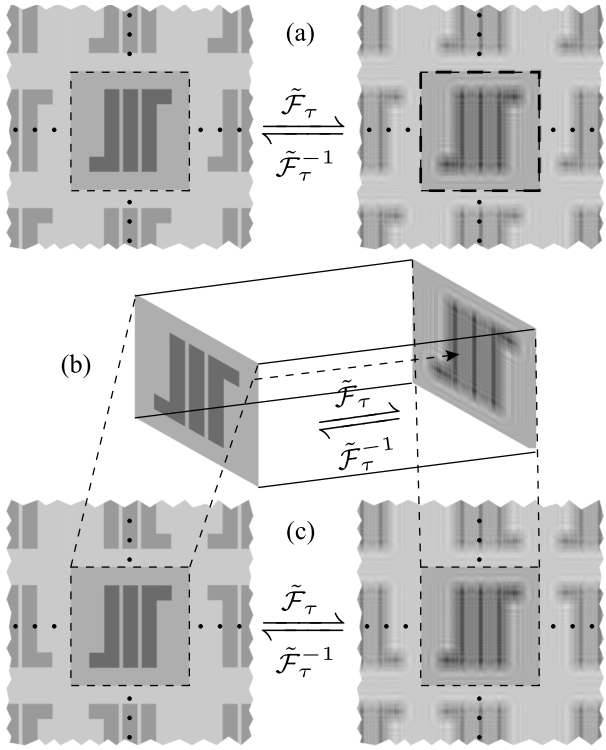

Fig. 2. Two boundary conditions discussed for discrete FrT: (a) periodic boundaries; (b) propagation of a finite-sized object/field confined within a rectangular waveguide lined with mirrors on its four interior planar surfaces, analogous to using (c) mirror-symmetric boundaries for the discrete transform.

the solutions to these problems in Subsections 3.B and 3.C, respectively.

A. Discrete Representation of Continuous Signals

We consider signals f in the Hilbert space L_2, which consists of all functions that are square-integrable in Lebesgue's sense. While we focus on 1D signals, extension to higher dimensions will be straightforward. We further consider SI subspaces of L_2, which are generated by scaled and shifted versions of a template function, φ_1, denoted as

$$V_1 = \left\{ f | f(x) = \sum_{k\in\mathbb{Z}} c[k] \cdot \varphi_1\left(\frac{x}{\Delta x_1} - k\right); \|c\|_{\ell_2} < \infty \right\}, \quad (14)$$

where $\|c\|_{\ell_2}^2 \triangleq \sum_{k\in\mathbb{Z}} |c[k]|^2$. Any function $f \in L_2$ can be orthogonally projected onto such an SI subspace, to yield an optimal approximation [6], f^{V_1}, given by

$$f^{V_1}(x) = \frac{1}{\Delta x_1} \sum_{k\in\mathbb{Z}} \left\langle f, \varphi_1\left(\frac{\bullet}{\Delta x_1} - k\right) \right\rangle \cdot \varphi_1\left(\frac{x}{\Delta x_1} - k\right) \quad (15)$$

$$= \sum_{k\in\mathbb{Z}} c[k] \cdot \varphi_1\left(\frac{x}{\Delta x_1} - k\right), \quad (16)$$

where $\langle a, b \rangle = \int_{-\infty}^{\infty} a(\xi) b^*(\xi) \mathrm{d}\xi$ denotes an inner product and φ_1 is the dual of the template function φ_1, the integer-shifted versions of which span the same space V_1 and also satisfy the biorthogonality condition,

$$\langle \mathring{\varphi}_1(\bullet - m), \varphi_1(\bullet - n)\rangle = \delta[m-n], \qquad m,n \in \mathbb{Z}. \tag{17}$$

The frequency response of the dual basis is given by [23]

$$\hat{\mathring{\varphi}}_1(\nu) = \frac{\hat{\varphi}_1(\nu)}{\sum_{k\in\mathbb{Z}}|\hat{\varphi}_1(\nu+k)|^2}. \tag{18}$$

We note that $f^{V_1}(x) = f(x)$, if $f \in V_1$. Moreover, the orthogonal projection is completely characterized by the discrete sequence $c[k]$, as long as φ_1 forms a Riesz basis [6], which effectively guarantees the denominator in Eq. (18) is positive and bounded.

Possible basis functions include the sinc function from classical sampling theory, with $\mathring{\varphi}_1(x) = \varphi_1(x) = \mathrm{sinc}(x)$, where V_1 then corresponds to the subspace of L_2 that encompasses functions band-limited by $1/(2\Delta x_1)$ and $c[k]$ refers to signal samples after the band-limiting operation. Alternatively, to represent signals with finite support, B-splines are a possible choice [24,25]. The B-spline of degree n is defined as

$$\beta^n(x) = \underbrace{\beta^0 \star \beta^0 \star \cdots \star \beta^0}_{n+1 \text{ terms}}(x), \tag{19}$$

where $\beta^0(x) = \mathrm{rect}(x)$ from Eq. (13), using which its frequency response can be deduced as $\hat{\beta}^n(\nu) = \mathrm{sinc}^{n+1}(\nu)$. For a continuous signal that lies in a B-spline space, the coefficients $c[k]$ can be efficiently computed from its samples, $f^{V_1}[k] = f^{V_1}(k\Delta x_1)$, via recursive filtering [24].

B. Discretization of Continuous Convolution

We now show that continuous convolutions of the form

$$\tilde{g}(x) = f^{V_1} \star h(x), \tag{20}$$

can be numerically computed without aliasing, even in cases where f^{V_1} is not band-limited. With $f^{V_1}(x)$ fully characterized by the discrete sequence $c[k]$, we also wish to represent $\tilde{g}(x)$ using a similar discrete sequence and therefore approximate $\tilde{g}$ via an orthogonal projection onto an SI space, $V_2 = \mathrm{span}\{\varphi_2(\bullet/\Delta x_2 - k)\}_{k\in\mathbb{Z}}$, to obtain

$$\tilde{g}^{V_2}(x) = \sum_{k\in\mathbb{Z}} d[k]\cdot\varphi_2\left(\frac{x}{\Delta x_2} - k\right). \tag{21}$$

This pipeline of operations is illustrated in Fig. 3(a). Despite $f^{V_1}(x)$ and $\tilde{g}^{V_2}(x)$ being both functions of the continuous variable x, they are uniquely characterized by the discrete sequences $c[k]$ and $d[k]$, respectively. Remarkably, when the ratio between their sampling steps is rational, $\Delta x_2/\Delta x_1 = p/q$ $(p,q \in \mathbb{N})$, the sequences $c[k]$ and $d[k]$ are related via a discrete convolution with a digital filter, $u[k]$, shown in Fig. 3(b), whose exact expression we introduce in the following theorem.

■Theorem 1 (Equivalent digital filter for continuous convolutions): Let $f^{V_1}(x) = \sum_{k\in\mathbb{Z}} c[k]\cdot\varphi_1(x/\Delta x_1 - k)$, $\tilde{g}(x) = f^{V_1}\star h(x)$, and $d[k] = (\Delta x_2)^{-1}\cdot\langle \tilde{g}, \mathring{\varphi}_2(\bullet/\Delta x_2 - k)\rangle$, with $\Delta x_2/\Delta x_1 = p/q$ $(p,q\in\mathbb{N})$. Then, we have

$$d[k] = \sum_{\ell\in\mathbb{Z}} c[\ell]\cdot u[pk - q\ell], \tag{22}$$

where

$$u(x) = \frac{1}{\Delta x_2}\left\{\varphi_1\left(\frac{x}{\Delta x_1}\right)\star h(x)\star\mathring{\varphi}_2^*\left(-\frac{x}{\Delta x_2}\right)\right\}, \tag{23}$$

$$u[k] = u(k\Delta x_2/p). \tag{24}$$

Proof: The expression of u can be graphically derived in Figs. 3(a) and 3(b). □

When the input function is periodic, the discrete convolution in Eq. (22) simplifies to a circular convolution that can be implemented using FFT, leading to a generalized CV-FFT algorithm (GCV-FFT).

■Theorem 2 [FFT algorithm for computing continuous convolutions (GCV-FFT)]: Let $f^{V_1}(x) = \sum_{k\in\mathbb{Z}} c[k]\cdot\varphi_1(x/\Delta x_1 - k)$ be an $N\Delta x_1$-periodic function $(N\in\mathbb{N})$ and let $h(x)$ be a stable filter with known frequency response $\hat{h}(\nu)$. Then, the orthogonal projection of the continuous convolution $\tilde{g}(x) = f^{V_1}\star h(x)$ in an SI space V_2, $\tilde{g}^{V_2}(x) = \sum_{k\in\mathbb{Z}} d[k]\cdot\varphi_2(x/\Delta x_2 - k)$, with $\Delta x_2/\Delta x_1 = p/q$

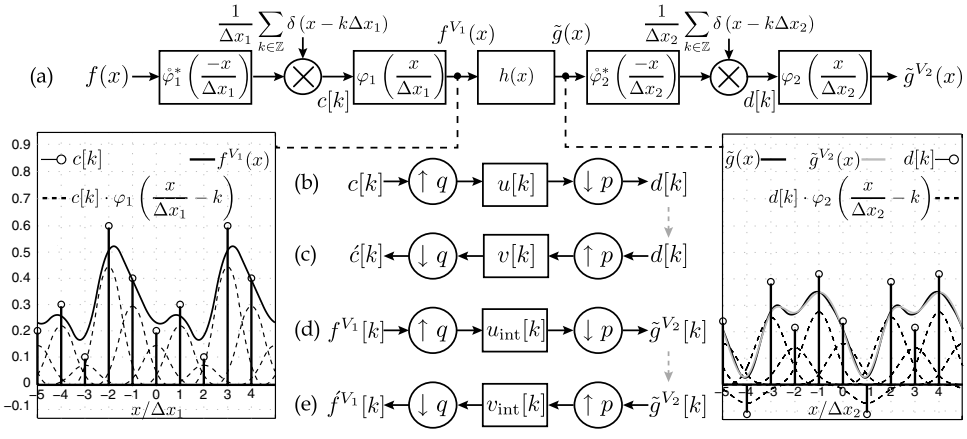

Fig. 3. Discretization of continuous convolution operations based on generalized sampling theory. (a) The continuous convolution $g(x) = f\star h(x)$ can be approximated using two suitable SI spaces, $V_i = \mathrm{span}\{\varphi_i(\bullet/\Delta x_i - k)\}_{k\in\mathbb{Z}}$, $(i = 1,2)$, as $\tilde{g}^{V_2}(x) = (f^{V_1}\star h)^{V_2}(x)$, which in turn can be numerically computed by a discrete convolution without aliasing, even when f and h are not band-limited. (b), (c) When $\Delta x_2/\Delta x_1 = p/q$, $(p,q\in\mathbb{N})$, the expansion coefficients of f^{V_1} and $\tilde{g}^{V_2}$ are related by digital filters for both (b) the forward and (c) the inverse convolution operation. (d), (e) Equivalent filters to (b) and (c) when the signals are defined by their discrete samples rather than expansion coefficients.

$(p, q, Nq/p \in \mathbb{N})$, is completely characterized by the discrete relation between $d[k]$ and $c[k]$:

$$d[k] = (1/p) \cdot \mathcal{F}^{-1}_{Nq/p}\{\mathcal{F}_N(c) \times U\}[k], \qquad 0 \le k < Nq/p, \quad (25)$$

where

$$U[k_0] = q \sum_{m\in\mathbb{Z}} \hat{\varphi}_1\left(\frac{k_0}{N} - mq\right) \cdot \hat{h}\left(\frac{k_0}{N\Delta x_1} - \frac{mq}{\Delta x_1}\right) \cdot \mathring{\hat{\varphi}}_2^*\left(\frac{pk_0}{Nq} - mp\right), \qquad 0 \le k_0 < Nq. \quad (26)$$

Proof: In Appendix A. □

Note that the N-periodic $\mathcal{F}_N(c)$ is concatenated with its copies to have length Nq, before its point-wise multiplication with the Nq-periodic vector U. The Nq-periodic product vector is then made to fold (alias), with every pth alternate element added together, changing its periodicity to Nq/p, before computing its Nq/p-point inverse FFT (IFFT). In practice, the infinite sum in Eq. (26) can be truncated to reach any desired accuracy. Note that this infinite sum will converge if $\hat{h}$ is bounded and if the basis functions φ_1, φ_2 generate Riesz bases. An illustration of the discrete implementation of a 1D convolution operation using the above result is shown in Fig. 3(a).

The following corollary describes the special case when $\tilde{g}(x) = f^{V_1} \star h(x)$ is sampled without projection onto V_2.

▶*Corollary 2.1 (Equivalent digital filter linking input coefficients to samples of the continuous convolution)*: Discrete samples of the convolved signal $\tilde{g}[k] = \tilde{g}(k\Delta x_2)$ are obtained via

$$\tilde{g}[k] = (1/p) \cdot \mathcal{F}^{-1}_{Nq/p}\{\mathcal{F}_N(c) \times U^s\}[k], \qquad 0 \le k < Nq/p, \quad (27)$$

where U^s is the Nq-point vector $(0 \le k_0 < Nq)$,

$$U^s[k_0] = q \sum_{m\in\mathbb{Z}} \hat{\varphi}_1\left(\frac{k_0}{N} - mq\right) \cdot \hat{h}\left(\frac{k_0}{N\Delta x_1} - \frac{mq}{\Delta x_1}\right). \quad (28)$$

Proof: Substitute $\mathring{\hat{\varphi}}_2(\nu) = 1$ in Eq. (26). □

While the input signal f^{V_1} is uniquely defined by the coefficients $c[k]$, it may also be directly defined by its discrete samples. For this case, the following corollary provides a discrete relationship between the samples of f^{V_1} and $\tilde{g}^{V_2}$ via a digital filter, $u_{\text{int}}[k]$ [Fig. 3(d)].

▶*Corollary 2.2 (Equivalent digital filter linking input–output samples of the continuous convolution)*: If $f \in V_1$ and $f[k] = f(k\Delta x_1)$ are its uniform samples, then $\tilde{g}^{V_2}[k] = \tilde{g}^{V_2}(k\Delta x_2)$, with $\Delta x_2/\Delta x_1 = p/q$, is given by

$$\tilde{g}^{V_2}[k] = (1/p) \cdot \mathcal{F}^{-1}_{Nq/p}\{\mathcal{F}_N(f) \times U^{\text{int}}\}[k], \qquad 0 \le k < Nq/p, \quad (29)$$

where U^{int} is the Nq-point vector,

$$U^{\text{int}}[k_0] = q \sum_{m\in\mathbb{Z}} \hat{\eta}_1\left(\frac{k_0}{N} - mq\right) \cdot \hat{h}\left(\frac{k_0}{N\Delta x_1} - \frac{mq}{\Delta x_1}\right) \cdot \mathring{\hat{\eta}}_2^*\left(\frac{pk_0}{Nq} - mp\right), \qquad 0 \le k_0 < Nq \quad (30)$$

with

$$\hat{\eta}_i(\nu) = \frac{\hat{\varphi}_i(\nu)}{\sum_{m\in\mathbb{Z}} \hat{\varphi}_i(\nu + m)}, \qquad i = 1, 2, \quad (31)$$

$$\mathring{\hat{\eta}}_i(\nu) = \frac{\hat{\varphi}_i(\nu) \cdot (\sum_{m\in\mathbb{Z}} \hat{\varphi}_i^*(\nu + m))}{\sum_{n\in\mathbb{Z}} |\hat{\varphi}_i(\nu + n)|^2}. \quad (32)$$

Proof: Since $f \in V_1, f(x) = f^{V_1}(x)$ and can be represented as in Eq. (16), with $c[k]$ and φ_1 replaced by $f[k]$ and η_1, respectively, where η_1 is the equivalent interpolating (i.e., $\eta_1(k) = \delta[k], k \in \mathbb{Z}$) basis function that also spans V_1 [23]. Similarly, $\tilde{g}^{V_2}(x)$ can also be represented using $\tilde{g}^{V_2}[k]$ and η_2. The FFT of the digital filter $u_{\text{int}}[k]$ is then found by replacing $\hat{\varphi}_1$ and $\mathring{\hat{\varphi}}_2$ in Eq. (26) by $\hat{\eta}_1$ and $\mathring{\hat{\eta}}_2$, respectively. Note that the discrete samples $\tilde{g}[k]$ can also be directly obtained from $f[k]$, using Eq. (29), by substituting $\mathring{\hat{\eta}}_2(\nu) = 1$ in Eq. (30). □

The number of computations required to carry out the discrete convolution in Theorem 2 can be further reduced when the signals involved have symmetries. In what follows, we distinguish between discrete periodic signals with *whole-sample* (WS) and *half-sample* (HS) mirror symmetry [26]. Such signals are mirror-symmetric about a sample and about a point midway between two samples, respectively. HS mirror-symmetric boundary conditions are illustrated in Figs. 2(b) and 2(c).

▶*Corollary 2.3 (Low complexity FFT algorithm for continuous convolution of signals with mirror symmetry)*: Let $f^{V_1}(x) = \sum_{k\in\mathbb{Z}} c^{\text{m}}[k] \cdot \varphi_1(x/\Delta x_1 - k)$, with c^{m} being a $2N$-point periodic sequence having HS mirror symmetry,

$$c^{\text{m}}[k] = \begin{cases} c[k], & 0 \le k < N \\ c[2N - 1 - k], & N \le k < 2N. \end{cases} \quad (33)$$

If $u(x) = u(-x)$ in Eq. (23) and $\Delta x_1 = \Delta x_2$, then we have $\tilde{g}^{V_2}(x) = \sum_{k\in\mathbb{Z}} d^{\text{m}}[k] \cdot \varphi_2(x/\Delta x_1 - k)$, where $d^{\text{m}}[k]$ is also a $2N$-point sequence with HS mirror symmetry. Furthermore, the even and odd elements of its corresponding N-point first-half, $d[k]$, are given by

$$d[2k] = d^{\text{m}}[2k] \triangleq d^{\text{m}}_{\text{even}}[k], \qquad 0 \le k < \lceil N/2 \rceil, \quad (34)$$

$$d[2k + 1] = d^{\text{m}}_{\text{even}}[N - 1 - k], \qquad 0 \le k < \lceil (N - 1)/2 \rceil, \quad (35)$$

where

$$d^{\text{m}}_{\text{even}}[k] = \mathcal{F}^{-1}_N\left\{\frac{\mathcal{F}_{2N}\{d^{\text{m}}\}[\circ] + \mathcal{F}_{2N}\{d^{\text{m}}\}[\circ + N]}{2}\right\}[k], \quad (36)$$

for $0 \le k < N$, and

$$\mathcal{F}_{2N}\{d^{\text{m}}\}[k_0] \triangleq \mathcal{F}_{2N}\{c^{\text{m}}\}[k_0] \times U^{\text{m}}, \qquad 0 \le k_0 < 2N, \quad (37)$$

$$\mathcal{F}_{2N}\{c^{\text{m}}\}[k_0] = \mathcal{F}_N\{c^{\text{m}}_{\text{even}}\}[k_0] + \left\{\exp\left(j\frac{\pi}{N}k_0\right) \cdot \mathcal{F}_N\{c^{\text{m}}_{\text{even}}\}[N - k_0]\right\}, \quad (38)$$

$$U^{\mathrm{m}}[k_0] = \sum_{m\in\mathbb{Z}} \hat{\varphi}_1\left(\frac{k_0}{2N} - m\right) \cdot \hat{h}\left(\frac{k_0}{2N\Delta x_1} - \frac{m}{\Delta x_1}\right) \cdot \hat{\mathring{\varphi}}_2^{*}\left(\frac{k_0}{2N} - m\right). \tag{39}$$

Proof: When $c[k]$ and $u[k]$ have HS and WS symmetry, respectively, $d[k] = c * u[k]$ has HS symmetry [26]. The mirror symmetry in the input and output signals thereby allows their FFT/IFFT to be computed using half-length counterparts [27]. Note that Eq. (39) is exactly similar to Eq. (26), with N replaced by $2N$ and $p = q = 1$. □

It follows that if φ_1, φ_2 have even symmetry (e.g., B-splines), the stated requirement of $u(x) = u(-x)$ is satisfied if $h(x) = h(-x)$ (e.g., FrT). The fact that the calculations involve nonredundant signals of half and quarter the original size in the 1D and 2D cases, reduces the FFT/IFFT computational complexity involved by 50% and 75%, respectively.

C. Invertibility of the Equivalent Digital Filters

With GCV-FFT providing an efficient way to solve the forward problem (P1), we look next at the inverse problem (P2), to recover the samples of the original signal f^{V_1} from the measurements of $\tilde{g} = f^{V_1} \bigstar h$, obtained with a known acquisition device, using prior information about h and the SI space in which f^{V_1} lies. We refer to this as the inverse GCV-FFT (IGCV-FFT) algorithm, corresponding to a continuous filter, h.

Invertibility is particularly important in digital systems [28] and has been investigated for Fresnel-like transforms before [29,30]. Here, we seek a sequence $c'[k]$ whose forward transform closely matches $d[k]$ in the least-squares sense. In the following theorem, we prove that the coefficients $c'[k]$ can be obtained from $d[k]$ by applying a digital filter, $v[k]$ [Fig. 3(c)], and provide its FFT coefficients.

▪Theorem 3 (IGCV-FFT algorithm for discrete inverse convolution): Let the Nq/p-periodic coefficients $d[k]$ result from the forward convolution in Theorem 2, $d[k] = \sum_{l\in\mathbb{Z}} c[l] \cdot u[pk - ql]$. Then the sequence c' with minimum ℓ_2-norm that minimizes the problem

$$c' = \arg\min_{c\in\ell_2} \left\| d - \sum_{l\in\mathbb{Z}} c[l] \cdot u[p \bullet -ql] \right\|_{\ell_2} \tag{40}$$

is obtained through the linear filtering operation,

$$c'[k] = (1/q) \cdot \mathcal{F}_N^{-1}\{\mathcal{F}_{Nq/p}(d) \times V\}[k], \qquad 0 \le k < N, \tag{41}$$

where

$$V[k_0] = pq\mathbf{U}^{\dagger}_{k_0 \bmod N}[0, \lfloor k_0/N \rfloor], \qquad 0 \le k_0 < Nq, \tag{42}$$

and $\mathbf{U}_r^{\dagger}$ denotes the Moore–Penrose pseudoinverse of the $q \times p$-sized matrix $\mathbf{U}_r$, defined as

$$\mathbf{U}_r[m,n] = U\left[r + Nm + \frac{Nq}{p}n\right], \qquad 0 \le m < q, 0 \le n < p \tag{43}$$

with U defined as in Eq. (26).

Proof: In Appendix B. □

When $\Delta x_1 = \Delta x_2$ ($p = q = 1$), the above result simplifies to $V[k_0] = 1/U[k_0]$, $0 \le k_0 \le N - 1$, for nonzero values of U, and zero otherwise. In particular, when $h = h_{\mathrm{FrT},\tau}$ is the FrT kernel and φ_1, φ_2 are chosen as B-spline functions with $\Delta x_1 = \Delta x_2$, the FFT coefficients $U[k_0]$ in Eq. (26) are always nonzero, thereby ensuring the possibility of perfect reconstruction. For arbitrary choices of φ_1, φ_2, Δx_1, Δx_2 and h, the minimum ℓ_2-norm solution yields perfect reconstruction, if and only if the $q \times p$ matrices in Eq. (43) are full-rank matrices, with their rank equal to p. A similar inverse to Corollary 2.2 is straightforward in this context, where $f'^{V_1}[k] = f'^{V_1}(k\Delta x_1)$, $f'^{V_1}(x) = \sum_{k\in\mathbb{Z}} c'[k] \cdot \varphi_1(x/\Delta x_1 - k)$, can be obtained from $\tilde{g}^{V_2}[k]$ using a digital filter, $v_{\mathrm{int}}[k]$, shown in Fig. 3(e), whose FFT coefficients V^{int} can be obtained from Eq. (42), with U in Eq. (43) replaced by U^{int} of Eq. (30).

4. APPLICATION TO DIGITAL HOLOGRAPHY

We now derive discrete filters for the Rayleigh–Sommerfeld diffraction integral and the FrT. This is achieved by replacing the continuous filter h in the expression for the digital filter $u[k]$, derived in Eq. (24) of Theorem 1, by $h_{\mathrm{RS},\lambda,z}$ and $h_{\mathrm{FrT},\tau}$ (or $h_{\mathrm{FrA},\lambda,z}$), respectively. The 2D FFT coefficients of the digital filter corresponding to the Rayleigh–Sommerfeld diffraction integral can be thus obtained by extending Eq. (26) to 2D as follows:

$$\begin{aligned} U^{\mathrm{RS}}[k_0, l_0] = q_x q_y \sum_{m,n\in\mathbb{Z}} \Bigg\{ & \hat{\varphi}_1\left(\frac{k_0 - mN_x q_x}{N_x}, \frac{l_0 - nN_y q_y}{N_y}\right) \\ & \cdot \hat{h}_{\mathrm{RS},\lambda,z}\left(\frac{k_0 - mN_x q_x}{N_x \Delta x_1}, \frac{l_0 - nN_y q_y}{N_y \Delta y_1}\right) \\ & \cdot \hat{\mathring{\varphi}}_2^{*}\left(\frac{k_0 - mN_x q_x}{N_x q_x/p_x}, \frac{l_0 - nN_y q_y}{N_y q_y/p_y}\right) \Bigg\}, \end{aligned} \tag{44}$$

for $0 \le k_0 < N_x q_x$, $0 \le l_0 < N_y q_y$, where $\Delta x_2/\Delta x_1 = p_x/q_x$, $\Delta y_2/\Delta y_1 = p_y/q_y$. Similarly, the 1D FFT coefficients of the digital filter corresponding to the separable and unitary FrT can be deduced as

$$\begin{aligned} U^{\mathrm{FrT}}[k_0] = q \sum_{m\in\mathbb{Z}} \Bigg\{ & \hat{\varphi}_1\left(\frac{k_0 - mNq}{N}\right) \cdot \hat{\mathring{\varphi}}_2^{*}\left(\frac{k_0 - mNq}{Nq/p}\right) \\ & \cdot \exp\left(j\frac{\pi}{4}\right) \cdot \exp\left(-j\pi\tau^2\left(\frac{k_0 - mNq}{N\Delta x_1}\right)^2\right) \Bigg\}, \end{aligned} \tag{45}$$

for $0 \le k_0 < Nq$. Note that the band-limited CV-FFT approach in Eq. (11) reduces to a special case of Eq. (45), where $\hat{\varphi}_1(\nu) = \hat{\varphi}_2(\nu) = \mathrm{rect}(\nu)$ and $\Delta x_1 = \Delta x_2$.

5. EXPERIMENTAL RESULTS AND DISCUSSION

With the framework for the numerical implementation of convolution operations laid out in the previous sections, we now illustrate its features and practical applicability, via simulation results.

A. Inverse Transform from Sampled Fresnel Integral

Here, we compare the reconstruction fidelity for CV-FFT and IGCV-FFT, by individually estimating a signal from its FrT samples, where the latter is originally calculated using the more computationally intensive and accurate Fresnel integrals [2]. We consider a box signal, $f(x)$, with aperture width $w = 5.15$ mm, composed of $N = 4096$ samples, spaced apart

by $\Delta x_1 = 10$ μm [Fig. 1(a)]. We use a box function as the reference since its FrT can be numerically computed using Fresnel integrals in an accurate manner. Using a C implementation of the integral [22], we obtain the FrT samples $\tilde{f}_\tau(k\Delta x_1)$, with $\tau = (\lambda z)^{0.5}$ given by $\lambda = 632$ nm and $z = 5$ mm, as in Fig. 1(b). We then estimate $f(k\Delta x_1)$ from $\tilde{f}_\tau(k\Delta x_1)$, using CV-FFT and IGCV-FFT.

While the inverse FrT computed with CV-FFT can be seen to suffer from Gibbs oscillations [Fig. 1(c)], the reconstruction obtained using IGCV-FFT [with $\varphi_1(x) = \beta^0(x)$, $h(x) = h_{\mathrm{FrT},\tau}(x)$, $\varphi_2(x) = \delta(x)$ and $\Delta x_1 = \Delta x_2$ in Eq. (26)] produces a more fair reconstruction [Fig. 1(d)].

B. Reconstruction of Non-Band-Limited Signals Leveraging *a Priori* Knowledge

We now illustrate how the knowledge that the recovered signal lies in a space V_1 can be exploited during inversion using IGCV-FFT. We consider the signal $f(x)$ shown in Fig. 4(a), defined as a linear combination of box, linear, and cubic B-splines. Due to the inherent linearity and shift-invariance of the system, the FrT samples of $f(x)$ are given by adding the output of three instances of GCV-FFT, where $\varphi_1(x) = \beta^i(x)$ and $\varphi_2(x) = \delta(x)$, for $i = 0, 1, 3$, respectively [Fig. 4(b)]. We then attempt to reconstruct $f(x)$ by alternately assuming that it lies in a band-limited space (which it does not) or in any one of the three different SI spaces $V_1 = \mathrm{span}\{\beta^i(\bullet - k)\}_{k\in\mathbb{Z}}$, $i = 0, 1, 3$ (which it does not either, since f is a combination of all three). The CV-FFT approach, in Fig. 4(c), suffers from severe ringing artifacts, particularly because none of the three basis functions constituting the input signal is similarly band-limited. Instead, using the inverse filter in Eq. (42) with $\varphi_1(x) = \beta^i(x)$, $\varphi_2(x) = \delta(x)$, and $\Delta x_1 = \Delta x_2$ for $i = 0, 1, 3$, the reconstructions are all ringing-free, yet they faithfully recover only those spatial regions of $f(x)$ that are well represented by the assumed reconstruction space V_1 [Figs. 4(d) and 4(f)].

C. Modeling of Acquisition Sensors with Finite Fill Factors

We next look at how GCV-FFT can naturally model the imaging process with digital cameras, where each sensor spatially averages the incoming signal over its active area [Fig. 5(a)] to give a pixel value. Note that this boils down to taking $\varphi_2(x) = \beta^0(x/\gamma)$ [Fig. 5(b)], with $d[k]$ then representing the pixel values. The corresponding dual basis is similarly defined as $\mathring{\varphi}_2(x) = (1/\gamma)\beta^0(x/\gamma)$, where $0 < \gamma \le 1$ is the fill factor [11], defined as the ratio between the integration area and the pixel size it represents.

As an example, we consider the FrT of a square aperture that is measured by its projection onto $V_{\mathrm{CCD}} = \mathrm{span}\{\varphi_2(\bullet/\Delta x_2 - k)\}_{k\in\mathbb{Z}}$, where $\varphi_2(x) = \beta^0(x/\gamma)$ [Fig. 5(c)]. Since the model underlying the CV-FFT reconstruction does not match the acquisition procedure, the band-limited reconstruction produces ringing artifacts. These artifacts can be visually highlighted as dark regions using the Structural Similarity Map (SSIM) [31], which associates a high index (1) to regions similar to the ground truth and a low index (0) to regions that differ, as shown in Fig. 5(e). Instead, by using $\varphi_1(x) = \beta^0(x)$, $h(x) = h_{\mathrm{FrT},\tau}(x)$, $\varphi_2(x) = \beta^0(x/\gamma)$, the IGCV-FFT algorithm is well adapted to the problem at hand and hence yields perfect reconstruction, as evident in Figs. 5(f) and 5(g).

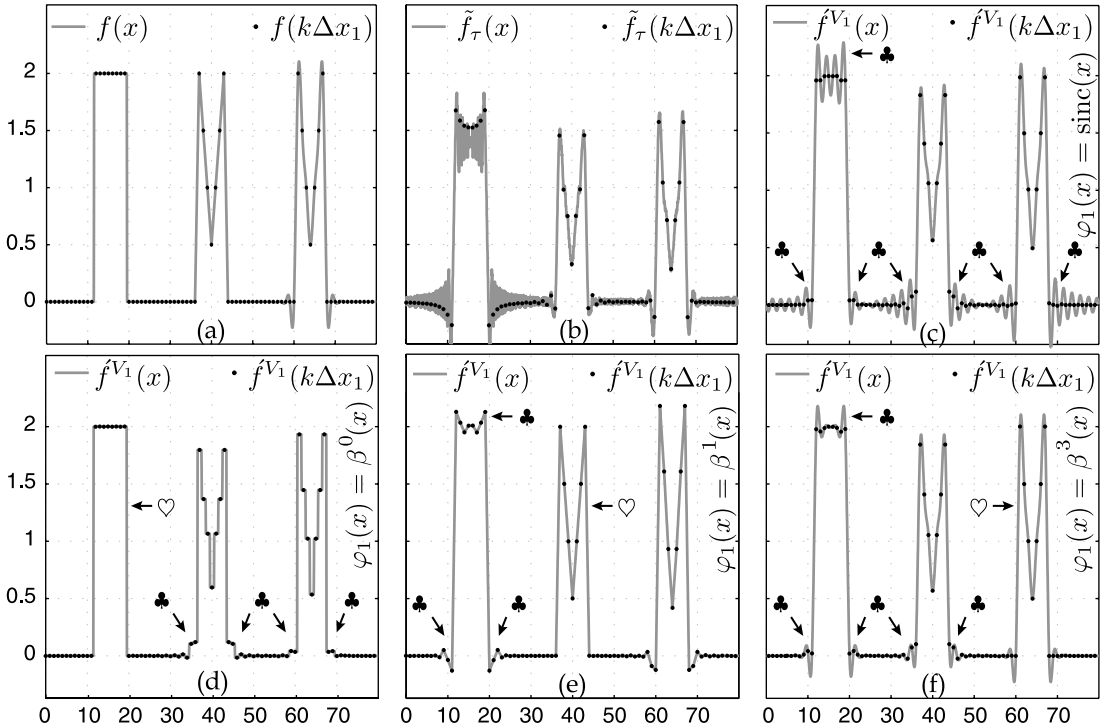

Fig. 4. (a) $f(x)$ composed of three types of basis functions (β^0, β^1, and β^3); (b) $\tilde{f}_\tau(x)$, where $\tau = 1$, (only real values shown) and its samples subsequently used for the recovery of $f(x)$; (c) the reconstructed signal and samples in the band-limited space, obtained using CV-FFT; (d)–(f) the recovered signal in the three separate SI spaces, $V_1 = \mathrm{span}\{\beta^i(\bullet - k)\}_{k\in\mathbb{Z}}$, $i = 0, 1, 3$, using IGCV-FFT. Clover leaves indicate reconstruction artifacts (e.g., Gibbs oscillation) and hearts denote perfect reconstruction.

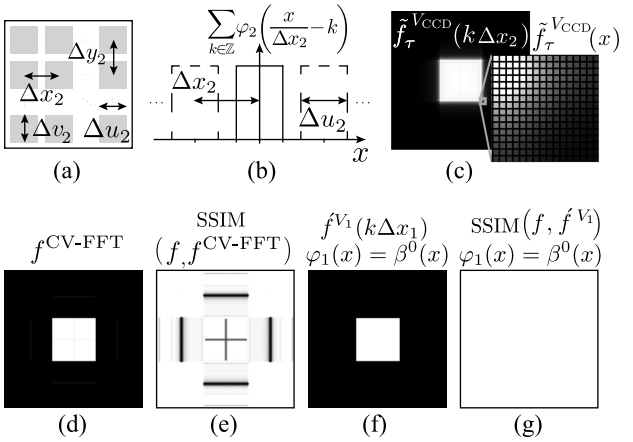

Fig. 5. (a) Typical CCD with finite-size detector elements and (b) its corresponding family of 1D basis functions. (c) $\tilde{f}^{V_{\mathrm{CCD}}}_{(\lambda\cdot z)^{0.5}}(k\Delta x_2)$ (only absolute values shown) ($\lambda = 632$ nm, $z = 1$ cm, $\Delta x_1 = \Delta x_2 = 10$ μm, $\gamma = 0.7$) for a square aperture, $f(x)$ (not shown). (d) Reconstruction using CV-FFT and (e) its SSIM map [31] showing the presence of artifacts (white: SSIM = 1, black: SSIM = 0). (f) Reconstruction using IGCV-FFT, yielding (g) an SSIM map that is uniformly 1 (white, perfect reconstruction).

In the particular context of digital holography, Stern and Javidi [11], and more recently Kelly and Claus [32], have shown that finite-size pixels attenuate high spatial frequencies in the propagated signal, in addition to the artifacts introduced by the sampling operation, rendering a perfect reconstruction virtually impossible. Here, we overcome this limitation by leveraging prior knowledge of the basis functions that underly the acquisition device and the signal.

D. Comparison of GCV-FFT for h^{-1} with IGCV-FFT for h

Since GCV-FFT allows discretizing forward convolutions with h, it could also be used to approximate the inverse operation h^{-1}. However, this is not equivalent to computing the IGCV-FFT algorithm for h. Specifically, for a signal $f \in V_1$, the sequence of operations consisting of (a) continuous convolution with h, (b) projection onto V_2, (c) continuous convolution with h^{-1}, and finally (d) projection onto V_1, is usually not identity.

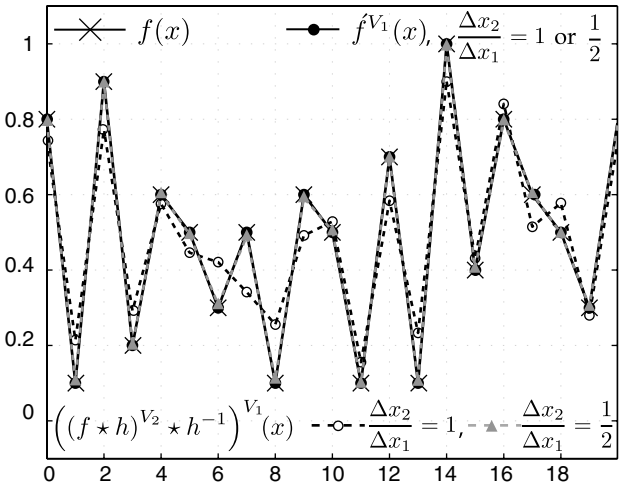

Fig. 6. Comparison of methods to estimate f from $\tilde{f}^{V_2}_{\tau}$ (not shown), where $\tau = 2.5$ and $\varphi_2 = \beta^1$, using *discrete-inverse* f^{V_1} with IGCV-FFT, and alternatively, using *discretized-continuous-inverse* $(\tilde{f}^{V_2}_{\tau} \star h^{-1}_{\mathrm{FrT},\tau})^{V_1}$ with GCV-FFT.

In order to illustrate the difference between using (i) GCV-FFT for h^{-1} and (ii) IGCV-FFT for h, we consider a signal $f \in V_1 = \mathrm{span}\{\beta^1(\bullet/\Delta x_1 - k)\}_{k\in\mathbb{Z}}$, as shown in Fig. 4. Using GCV-FFT, we compute its discretized FrT, $\tilde{f}^{V_2}_{\tau}$, measured via projection into $V_2 = \mathrm{span}\{\beta^1(\bullet/\Delta x_2 - k)\}_{k\in\mathbb{Z}}$, with $\Delta x_2/\Delta x_1 = 1$ or $1/2$. We then estimate f from $\tilde{f}^{V_2}_{\tau}$ using either approach and compare the reconstruction results. The reconstruction obtained using (i) differs from f, while (ii) proves to be a perfect reconstruction (Fig. 6). The quality of the reconstructed signal using (i) improves when $\Delta x_2/\Delta x_1 = 1/2$. The IGCV-FFT approach yields perfect reconstruction for both $\Delta x_2/\Delta x_1 = 1$ and $1/2$.

6. DISCUSSION AND CONCLUSION

By approximating input and output functions as linear combinations of localized basis functions we obtain a flexible framework to compute continuous convolutions. Its main features are summarized below: (i) it does not require assuming the input or output signals are band-limited thereby limiting Gibbs oscillation artifacts near sharp edges; (ii) it takes into account variable sampling rates between the input and output signals making it suitable for multiresolution algorithms [21,33]; (iii) the implementation retains the form of a discrete convolution, making it directly applicable wherever band-limited methods are in use; (iv) the basis functions can be chosen to match the experimental, camera-specific setups; (v) both periodic and mirror-periodic boundary conditions can be selected (with a fast algorithm for mirror-periodic signals that reduces the computational complexity by a factor of 2 (in 1D) and 4 (in 2D) over direct periodic implementation); and (vi) the equivalent discrete inverse operator, optimal in the least-squares sense, can be implemented using the same algorithm.

Our approach could be applied to a wide range of analog operators. Experiments to compute and reconstruct complex wave fields indicate that our approach might be particularly well suited for digital holography applications. To facilitate integration with existing methods (which could include recent compressed-sensing methods [34–36]) and spur new uses, we make Matlab code available [37].

APPENDIX A: PROOF OF THEOREM 2

The frequency response of the digital filter in Eq. (24) is

$$U(e^{j2\pi\nu\Delta x_1/q}) = q\sum_{m\in\mathbb{Z}}\left\{\hat{\varphi}_1(\Delta x_1\nu - mq)\cdot\hat{h}\left(\nu - \frac{mq}{\Delta x_1}\right)\cdot\mathring{\hat{\varphi}}^{*}_{2}(\Delta x_2\nu - mp)\right\}. \tag{A1}$$

The corresponding Nq-point FFT vector is obtained by sampling Eq. (A1) at $\Delta\nu = 1/(N\Delta x_1)$, yielding the expression in Eq. (26).

APPENDIX B: PROOF OF THEOREM 3

We denote by $\mathbf{c}$ and $\mathbf{d}$ the column vectors that contain the N input and Nq/p output coefficients in GCV-FFT:

$$\mathbf{d} = \mathbf{A}\cdot\mathbf{c}, \tag{B1}$$

where the transformation matrix $\mathbf{A}$ is given by

$$\mathbf{A} = \mathbf{W}_{Nq/p}^{-1} \cdot \mathbf{U} \cdot \mathbf{W}_N, \tag{B2}$$

$$\mathbf{U} = \begin{bmatrix} \mathbf{I}_{Nq/p} & \mathbf{I}_{Nq/p} \end{bmatrix} \cdot \mathcal{D}_U \cdot \begin{bmatrix} \mathbf{I}_N \\ \vdots \\ \mathbf{I}_N \end{bmatrix}, \tag{B3}$$

$$\mathbf{W}_N[m,n] = \exp(-j2\pi mn/N), \qquad 0 \le m,n < N, \tag{B4}$$

$$\mathcal{D}_U[m,n] = U[m] \cdot \delta[m-n], \qquad 0 \le m,n < Nq, \tag{B5}$$

$$\mathbf{I}_N[m,n] = \delta[m-n], \qquad 0 \le m,n < N, \tag{B6}$$

so that $\mathrm{rank}(\mathbf{A}) = \mathrm{rank}(\mathbf{U})$. It can be verified that $\mathbf{U}$ is a sparse matrix having only the Nq FFT coefficients in $\mathcal{D}_U$ as its nonzero entries, and that

$$\mathrm{rank}(\mathbf{U}) = \sum_{r=0}^{N/p-1} \mathrm{rank}(\mathbf{U}_r), \tag{B7}$$

where $\mathbf{U}_r$ is as given in Eq. (43). This allows the pseudoinverse [28] of $\mathbf{U}$ to be calculated from smaller matrices $\mathbf{U}_r$. The pseudoinverse of $\mathbf{A}$ is given by

$$\mathbf{A}^\dagger = \mathbf{W}_N^{-1} \cdot \mathbf{U}^\dagger \cdot \mathbf{W}_{Nq/p}, \tag{B8}$$

and has essentially the same form as Eq. (B2), involving up-sampling, convolution, and down-sampling operations.

ACKNOWLEDGMENTS

M. L. was supported by a Hellman Faculty Fellowship.

REFERENCES

1. M. Born and E. Wolf, *Principles of Optics: Electromagnetic Theory of Propagation, Interference and Diffraction of Light*, 7th ed. (Cambridge University, 1999).
2. J. W. Goodman, *Introduction to Fourier Optics*, 2nd ed. (McGraw-Hill, 1996).
3. L. P. Yaroslavskii and N. S. Merzlyakov, *Methods of Digital Holography* (Consultants Bureau, 1980).
4. J. W. Goodman and R. W. Lawrence, "Digital image formation from electronically detected holograms," Appl. Phys. Lett. **11**, 77–79 (1967).
5. C. E. Shannon, "Communication in the presence of noise," Proc. IRE **37**, 10–21 (1949).
6. M. Unser, "Sampling-50 years after Shannon," Proc. IEEE **88**, 569–587 (2000).
7. M. Unser, "A general Hilbert space framework for the discretization of continuous signal processing operators," Proc. SPIE **2569**, 51–61 (1995).
8. S. Horbelt, M. Liebling, and M. Unser, "Discretization of the Radon transform and of its inverse by spline convolutions," IEEE Trans. Med. Imaging **21**, 363–376 (2002).
9. F. Gori, "Fresnel transform and sampling theorem," Opt. Commun. **39**, 293–297 (1981).
10. L. Onural, "Sampling of the diffraction field," Appl. Opt. **39**, 5929–5935 (2000).
11. A. Stern and B. Javidi, "Analysis of practical sampling and reconstruction from Fresnel fields," Opt. Eng. **43**, 239–250 (2004).
12. K. Matsushima and T. Shimobaba, "Band-limited angular spectrum method for numerical simulation of free-space propagation in far and near fields," Opt. Express **17**, 19662–19673 (2009).
13. A. Stern and B. Javidi, "Sampling in the light of Wigner distribution," J. Opt. Soc. Am. A **21**, 360–366 (2004).
14. B. M. Hennelly and J. T. Sheridan, "Generalizing, optimizing, and inventing numerical algorithms for the fractional Fourier, Fresnel, and linear canonical transforms," J. Opt. Soc. Am. A **22**, 917–927 (2005).
15. J. J. Healy and J. T. Sheridan, "Sampling and discretization of the linear canonical transform," Signal Process. **89**, 641–648 (2009).
16. T. M. Kreis, M. Adams, and W. P. O. Jueptner, "Methods of digital holography: a comparison," Proc. SPIE **3098**, 224–233 (1997).
17. D. Mendlovic, Z. Zalevsky, and N. Konforti, "Computation considerations and fast algorithms for calculating the diffraction integral," J. Mod. Opt. **44**, 407–414 (1997).
18. D. Mas, "Fast algorithms for free-space diffraction patterns calculation," Opt. Commun. **164**, 233–245 (1999).
19. F. Zhang, I. Yamaguchi, and L. P. Yaroslavsky, "Algorithm for reconstruction of digital holograms with adjustable magnification," Opt. Lett. **29**, 1668–1670 (2004).
20. P. Ferraro, S. D. Nicola, G. Coppola, A. Finizio, D. Alfieri, and G. Pierattini, "Controlling image size as a function of distance and wavelength in Fresnel-transform reconstruction of digital holograms," Opt. Lett. **29**, 854–856 (2004).
21. M. Liebling, T. Blu, and M. Unser, "Fresnelets: new multiresolution wavelet bases for digital holography," IEEE Trans. Image Process. **12**, 29–43 (2003).
22. W. H. Press, S. A. Teukolsky, W. T. Vetterling, and B. P. Flannery, *Numerical Recipes in C: The Art of Scientific Computing*, 2nd ed. (Cambridge University, 1992).
23. T. Blu and M. Unser, "Quantitative Fourier analysis of approximation techniques: part I-Interpolators and projectors," IEEE Trans. Signal Process. **47**, 2783–2795 (1999).
24. M. Unser, "Splines: a perfect fit for signal and image processing," IEEE Signal Process. Mag. **16**, 22–38 (1999).
25. E. Cuche, P. Marquet, and C. Depeursinge, "Aperture apodization using cubic spline interpolation: application in digital holographic microscopy," Opt. Commun. **182**, 59–69 (2000).
26. C. M. Brislawn, "Classification of nonexpansive symmetric extension transforms for multirate filter banks," Appl. Comput. Harmon. Anal. **3**, 337–357 (1996).
27. A. Fertner, "Computationally efficient methods for analysis and synthesis of real signals using FFT and IFFT," IEEE Trans. Signal Process. **47**, 1061–1064 (1999).
28. M. Bertero and P. Boccacci, *Introduction to Inverse Problems in Imaging* (IOP, 1998).
29. I. Aizenberg and J. Astola, "Discrete generalized Fresnel functions and transforms in an arbitrary discrete basis," IEEE Trans. Signal Process. **54**, 4261–4270 (2006).
30. V. Katkovnik, A. Migukin, and J. Astola, "Backward discrete wave field propagation modeling as an inverse problem: toward perfect reconstruction of wave field distributions," Appl. Opt. **48**, 3407–3423 (2009).
31. Z. Wang, A. Bovik, H. Sheikh, and E. Simoncelli, "Image quality assessment: from error visibility to structural similarity," IEEE Trans. Image Process. **13**, 600–612 (2004).
32. D. P. Kelly and D. Claus, "Filtering role of the sensor pixel in Fourier and Fresnel digital holography," Appl. Opt. **52**, A336–A345 (2013).
33. M. Liebling, "Fresnelab: sparse representations of digital holograms," Proc. SPIE **8138**, 81380I (2011).
34. A. F. Coskun, I. Sencan, T.-W. Su, and A. Ozcan, "Lensless wide-field fluorescent imaging on a chip using compressive decoding of sparse objects," Opt. Express **18**, 10510–10523 (2010).
35. M. M. Marim, M. Atlan, E. Angelini, and J.-C. Olivo-Marin, "Compressed sensing with off-axis frequency-shifting holography," Opt. Lett. **35**, 871–873 (2010).
36. Y. Rivenson, A. Stern, and B. Javidi, "Compressive Fresnel holography," J. Display Technol. **6**, 506–509 (2010).
37. http://sybil.ece.ucsb.edu/.